


Article

Automatic Control of a Mobile Manipulator Robot Based on Type-2 Fuzzy Sliding Mode Technique

Xin Xu ^{1,*}, Ahmed Shaker ^{2,*}  and Marwa S. Salem ^{3,4}¹ Department of Mechanical Engineering, Taiyuan Institute of Technology, Taiyuan 030008, China² Engineering Physics and Mathematics Department, Faculty of Engineering, Ain Shams University, Cairo 11566, Egypt³ Department of Computer Engineering, College of Computer Science and Engineering, University of Ha'il, Ha'il 55211, Saudi Arabia⁴ Department of Electrical Communication and Electronics Systems Engineering, Faculty of Engineering, Modern Science and Arts University (MSA), Cairo 12556, Egypt

* Correspondence: xux@tit.edu.cn (X.X.); ahmed.shaker@eng.asu.edu.eg (A.S.)

Abstract: In this paper, an automatic control method based on type-2 fuzzy sliding mode control for a mobile arm robot is presented. These types of robots have very complex dynamics due to the uncertainty of the arm parameters and the mobility of their base, so conventional control methods do not provide a suitable solution. The proposed method proves convergence with Lyapunov theory, and its convergence is mathematically guaranteed. A type-2 fuzzy system is responsible for approximating unmodulated dynamics, nonlinear terms, and uncertain parameters. In simulations, the performance of the proposed method with different situations, including uncertainty in arm parameters, uncertainty in mobile robot parameters (arm robot base), uncertainty in load, as well as indeterminacy in modeling have been applied. The comparison with two conventional controllers shows the efficiency and superiority of the proposed method.

Keywords: automatic control; mobile robot; type-2 fuzzy; sliding mode technique**MSC:** 93-08

Citation: Xu, X.; Shaker, A.; Salem, M.S. Automatic Control of a Mobile Manipulator Robot Based on Type-2 Fuzzy Sliding Mode Technique.

Mathematics **2022**, *10*, 3773. <https://doi.org/10.3390/math10203773>

Academic Editors: KUEN-SUAN CHEN, Chun-Min Yu and Tsang-Chuan Chang

Received: 10 September 2022

Accepted: 8 October 2022

Published: 13 October 2022

Publisher's Note: MDPI stays neutral with regard to jurisdictional claims in published maps and institutional affiliations.



Copyright: © 2022 by the authors. Licensee MDPI, Basel, Switzerland. This article is an open access article distributed under the terms and conditions of the Creative Commons Attribution (CC BY) license (<https://creativecommons.org/licenses/by/4.0/>).

1. Introduction

Today, the robotics industry is developing with high intensity and speed. Robots are divided into two general categories: arm and mobile. Stationary robotic arms have been considered in the industry due to their high capability. They can do repetitive tasks with high accuracy. Despite this advantage, their main weakness is the lack of movement. To perform tasks with wide access space, mobile robotic puzzle is used [1–5]. Among the applications of the planet robotic arm, we can mention the military robot lamb load robot, guard robot, and probe robot [6]. Two-wheeled mobile robots are a subset of non-holonomic mechanical systems. If the position of the moving parts depends on each other, the motion constraint is called holonomic. Otherwise, it is called non-holonomic. Non-holonomic mobile robots are controlled by a number of actuators less than the degrees of freedom [7,8]. Motion control and tracking are determined by the type of constraint. So far, many methods have been proposed to control the robot. Interaction between the skilled arm and the moving arm, the presence of holonomic and non-holonomic feeds, and the nonlinear function are among the features of the mobile robotic arm that control. Model-based control has been considered as the basis of control methods and plans, in which, assuming the system model, the control law is presented [9]. In this regard, workplace separation control is introduced in [10] and nonlinear feedback control is presented in [11]. In both methods, the effect of external disturbance is not seen. There are many problems in implementing model-based controllers. One of the most important issues is the dependence on the exact

model of the system. As the exact model is not available, it has uncertainty. The control of the controller or the uncertainty of the dynamic parameter is not mediated and the perturbation of the thorn is even raised. In addition, the complexity of the model makes the design of the controller difficult.

To deal with this problem, robust and adaptive control methods have been applied. Adaptive tracking control resistant to parametric uncertainty and external perturbation was presented in [12–15]. The control loop configuration involves two parts, kinematic and adaptive control. Adaptive tracking control of the workspace path in the presence of uncertainty and perturbation was presented in [16], which does not require a torque sensor to estimate external perturbations. In both methods, perturbation was considered as a linear combination of several parameters. Adaptive robust control to control robot ether movement with holonomic and non-holonomic constraints was proposed in [17], in which parametric uncertainty and external perturbation were considered. Adaptive energy movement control was performed with output feedback for the skilled mobile arm in [18], which is resistant to parametric and dynamic uncertainty. Moreover, to prevent sliding in the force control ring, a non-holonomic constraint between the wheels and the ground was employed.

Sliding mode control is used as an effective method for the robust control of nonlinear systems. The problem with this method is the high frequency of the control signal, which stimulates unmodulated dynamics [19–22]. In the adaptive sliding mode control based on the backstepping method, the adaptive backstepping control is used to deal with the parametric uncertainty and the sliding mode method is used to deal with the limited disturbance. In contrast, fuzzy control has received more attention in recent years due to its ability to deal with uncertainty and simple design. The advantage of the fuzzy control method over conventional control methods is the ability to use language rules to employ experienced people [23]. Fuzzy control, as a model-free method, is simply used to control complex systems [24]. The ability to deal with fuzzy system uncertainties is improved by the law of adaptation [25]. In this respect, Lyapunov's direct method is used to design adaptive fuzzy control [26]. The fuzzy system is also used as a nonlinear system estimator in adaptive fuzzy control [27].

In [28], adaptive neuro-fuzzy control was presented to control the skilled arm on a sloping surface that is resistant to external disturbance. Adaptive force/neuro-fuzzy position control was introduced for the cooperation of skilled mobile arms, in which several robots work together to move an object with an unknown geometry and the physical model with unknown dynamics is robust. In [29], adaptive fuzzy control of a wheeled robot is a combination of kinematic control and adaptive fuzzy control that models the dynamics of the system considering the motors. Moreover, a control method has been presented based on an adaptive agate network for open and moving bodies. The control output is composed of two parts, the linear control component and compensating fit, which was intended to deal with uncertainty and turbulence [30–32]. Most of the previous designs have a complex structure full of companions and depend on the system model. Type-2 systems are much stronger than fuzzy type-1 and have better performance [33–36]. These systems have been widely used in control engineering and in increasing the accuracy of the controller. Therefore, in this article, for the first time, a type-2 fuzzy system is utilized in the sliding mode control structure for a mobile manipulator robot. The novelties in this paper are as follows:

- Two-stage control design for mobile manipulator system
- Stability analysis of the control system
- Use trapezoidal type-2 fuzzy sets combined with sliding mode control

The control scheme proposed in this article consists of two sections: kinematic and dynamic control. The purpose of kinematic control is to calculate the optimal speed for the robot so that the robot can follow the desired path accurately (instantaneous position control). The purpose of the dynamic control is to track the desired speed provided by the new type-2 adaptive fuzzy design (instantaneous speed control). The innovation here lies

in compensating for the type-2 fuzzy system approximation error for free convergence of the desired path in the presence of uncertainty. The features of this control are simplicity in design, proper performance in tracking the desired path in the presence of certainty science, and the guarantee of stability. This control method includes type-2 fuzzy sliding mode control and adaptive linear control. The mortal sliding gain control law brings the system state vector closer to the equilibrium point, and the adaptive linear control law ensures convergence to the desired target. Control rules are durable against finite perturbation.

2. Mathematical Modeling

The wheeled mobile robotic arm consists of two parts: the skilled arm and movable wheel. The moving body has two active wheels and one inactive wheel [19,22]. Side and top views of the robot are presented in Figure 1a,b, respectively. The axle of the active wheels is located in the same direction. The axis of the wheels is located at a distance d from the center of the mass and b is the distance between each wheel and the centerline as displayed in Figure 1. In robot modeling, the inactive multi-directional front wheel is omitted.

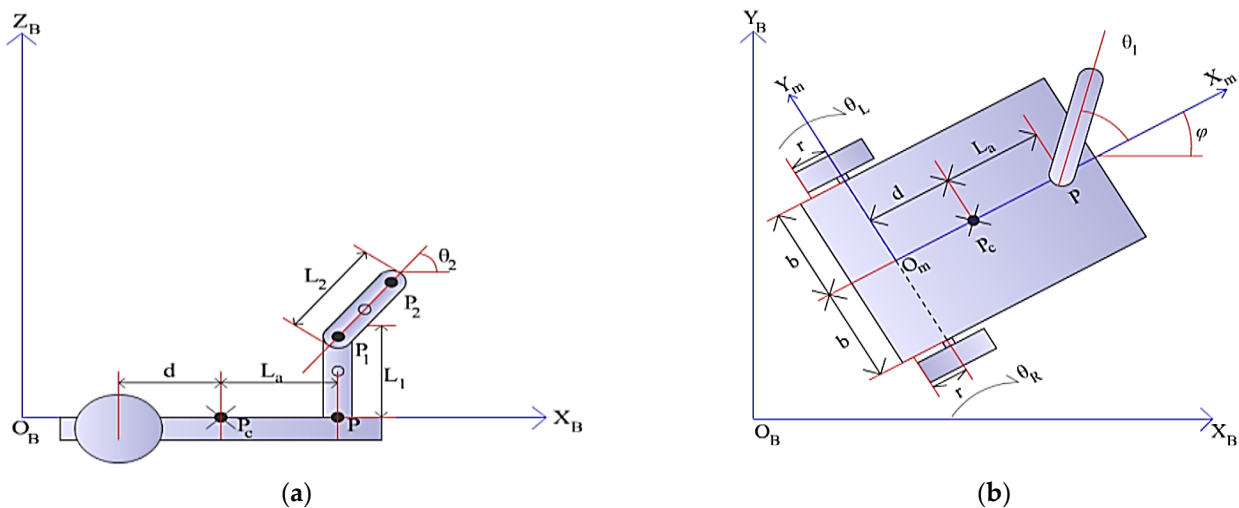


Figure 1. Schematic representation for the robot: (a) Side view and (b) Top view.

The $O_B X_B Y_B Z_B$ represents the base coordinate system and the $O_m X_m Y_m Z_m$ coordinate system is connected to the moving body. O_m is selected as the midpoint of the line connecting the two active wheels and the X_m axis is perpendicular to the line connecting the two active wheels.

The state vector is represented by $q_b = [x_c \ y_c \ \varphi \ \theta_R \ \theta_L]^T$, where x_c and y_c are the coordinates of the P_c point in the base coordinate system, φ is the angle of the X_m axis relative to the X_B axis and the variables θ_R and θ_L represent the right and left wheel rotation angles, respectively. Due to the position of the wheels and the assumption of complete rotation for them, the moving wheel drive in this robot has three movement constraints. The first non-holonomic constraint that prevents the wheels from moving along the Y_m axis is defined as follows

$$-\dot{x}_c \sin(\varphi) + \dot{y}_c \cos(\varphi) - d\dot{\varphi} = 0 \tag{1}$$

The other two constraints are related to the speed of the body and the speed of the wheels, which create non-sliding conditions for the wheels to roll completely along the X_m axis, namely:

$$\begin{aligned} \dot{x}_c \cos(\varphi) + \dot{y}_c \sin(\varphi) + b\dot{\varphi} &= r\dot{\theta}_R \\ \dot{x}_c \cos(\varphi) + \dot{y}_c \sin(\varphi) - b\dot{\varphi} &= r\dot{\theta}_L \end{aligned} \tag{2}$$

By connecting two rotating interfaces to the moving body at point P , a complete mobile gaming system is created. Its state vector is defined as follows:

$$\underline{q} = [x_c \ y_c \ \varphi \ \theta_R \ \theta_L \ \theta_1 \ \theta_2]^T \tag{3}$$

The variables θ_1 and θ_2 are the angle of the first interface with respect to the X_m and the angle of the second interface with respect to the $O_m X_m Y_m$, respectively. This can be written:

$$A(\underline{q})\dot{\underline{q}} = 0$$

$$A(\underline{q}) = \begin{bmatrix} -\sin(\varphi) & \cos(\varphi) & -d & 0 & 0 & 0 & 0 \\ -\cos(\varphi) & -\sin(\varphi) & -b & r & 0 & 0 & 0 \\ -\cos(\varphi) & -\sin(\varphi) & b & 0 & r & 0 & 0 \end{bmatrix} \tag{4}$$

According to Equation (4), there is a new state vector, \underline{v} , that establishes the following equations:

$$A(\underline{q})S(\underline{q}) = 0$$

$$\dot{\underline{q}} = S(\underline{q})\underline{v} \tag{5}$$

$$\underline{v} = [\dot{\theta}_R \ \dot{\theta}_L \ \dot{\theta}_1 \ \dot{\theta}_2]^T \in R^{N \times 1} (N = k - m)$$

where “ m ” is the dimensions of moving coordinates and is therefore equal to 3, and “ k ” is the state vector dimension of the system and is therefore equal to 7. Finally, N is the dimensions of the new state vector, which is equal to 4.

$$S(\underline{q}) = \begin{bmatrix} c(\text{bcos}(\varphi) - \text{dsin}(\varphi)) & c(\text{bcos}(\varphi) + \text{dsin}(\varphi)) & 0 & 0 \\ c(\text{bsin}(\varphi) + \text{dcos}(\varphi)) & c(\text{bsin}(\varphi) - \text{dcos}(\varphi)) & 0 & 0 \\ c & -c & 0 & 0 \\ 1 & 0 & 0 & 0 \\ 0 & 1 & 0 & 0 \\ 0 & 0 & 1 & 0 \\ 0 & 0 & 0 & 1 \end{bmatrix} \tag{6}$$

where $c = \frac{r}{2b}$.

The mechanical model of the robot is obtained using the Euler–Lagrange method. The Lagrangian $L(\underline{q}, \dot{\underline{q}})$ is defined as the difference between the kinetic energy and the potential energy of the system. Considering the torque of the motors as the input of the robot, we have the following equation,

$$\frac{d}{dt} \left(\frac{\partial L(\underline{q}, \dot{\underline{q}})}{\partial \dot{\underline{q}}} \right) - \frac{\partial L(\underline{q}, \dot{\underline{q}})}{\partial \underline{q}} = u \tag{7}$$

By solving the Euler–Lagrange equations, the dynamics of the robot become:

$$H_u(\underline{q})\ddot{\underline{q}} + V_u(\underline{q}, \dot{\underline{q}})\dot{\underline{q}} + G_u(\underline{q}) = E(\tau_i + \tau_{dis}(t)) - A^T(\underline{q})\underline{\lambda} \tag{8}$$

where $H_u(\underline{q}) \in R^{k \times k}$ is inertia matrix, $V_u(\underline{q}, \dot{\underline{q}}) \in R^{k \times k}$ is Coriolis force and centrifugal force, $G_u(\underline{q}) \in R^{k \times 1}$ is the gravitational force, $\tau_i \in R^{k \times 1}$ is the momentum of motion, $\tau_{dis}(t) \in R^{k \times 1}$ is the momentum of external turbulence, and $A^T(\underline{q})\underline{\lambda}$ are robot constraints. The matrix $E \in R^{k \times N}$ maps the torque vector to the variables of the joint space and the robot torque vector includes τ_R , the torque applied to the right wheel, τ_L , the torque applied

to the left wheel, τ_1 , the torque applied to the first rotating joint of the arm, and τ_2 , the torque applied to the second rotational joint of it.

$$\tau_i = [\tau_R \ \tau_L \ \tau_1 \ \tau_2]^T$$

$$E = \begin{bmatrix} 0 & 0 & 0 & 1 & 0 & 0 & 0 \\ 0 & 0 & 0 & 0 & 1 & 0 & 0 \\ 0 & 0 & 0 & 0 & 0 & 1 & 0 \\ 0 & 0 & 0 & 0 & 0 & 0 & 1 \end{bmatrix}^T \tag{9}$$

Multiplying the sides of Equation (6) in $S^T(\underline{q})$, the following equation is obtained,

$$S^T(\underline{q})H_u(\underline{q})\ddot{\underline{q}} + S^T(\underline{q})V_u(\underline{q},\dot{\underline{q}})\dot{\underline{q}} + S^T(\underline{q})G_u(\underline{q}) = S^T(\underline{q})E\tau_i + S^T(\underline{q})E\tau_{dis}(t) - S^T(\underline{q})A^T(\underline{q})\underline{\lambda} \tag{10}$$

For this robot, the matrices $S(\underline{q})$, $H_u(\underline{q})$, $V_u(\underline{q},\dot{\underline{q}})$, and $G_u(\underline{q})$ in Equation (10) are independent of the variables θ_L and θ_R , so we can write $S(\underline{q}_n)$, $H_u(\underline{q}_n)$, $V_u(\underline{q}_n,\dot{\underline{q}})$ and $G_u(\underline{q}_n)$, where $\underline{q}_n = [x_c \ y_c \ \varphi \ \theta_1]^T$.

Based on $S^T(\underline{q})A^T(\underline{q}) = 0$, the above equation becomes simpler.

$$\underline{H}(\underline{q}_n)\dot{\underline{v}} + \underline{C}(\underline{q}_n,\underline{v})\underline{v} + \underline{g}(\underline{q}_n) = \underline{\tau} + \underline{\tau}_d \tag{11}$$

In which,

$$\underline{H} = S^T(\underline{q}_n)H_u(\underline{q}_n)S(\underline{q}_n) \in R^{N \times N}, \tag{12}$$

$$\underline{C} = S^T(\underline{q}_n)H_u(\underline{q}_n)\dot{S} + S^T(\underline{q}_n)V_u(\underline{q}_n + S(\underline{q}_n)\underline{v})S(\underline{q}_n) \in R^{N \times N}, \tag{13}$$

$$\underline{g} = S^T(\underline{q}_n)G_u(\underline{q}_n) \in R^{N \times 1} \tag{14}$$

$$\underline{\tau} = S^T(\underline{q}_n)E\tau_i \in R^{N \times 1} \tag{15}$$

$$\underline{\tau}_d = S^T(\underline{q}_n)E\tau_{dis}(t) \in R^{N \times 1} \tag{16}$$

Note 1: The matrix \underline{H} is symmetric and positive definite.

Note 2: The $\underline{H} - 2\underline{C}$ matrix is nonsymmetric.

The robot state space model $X = [\underline{q} \ \underline{v}]^T$ is expressed as Equation (17).

$$\dot{X} = \begin{bmatrix} S(\underline{q})\underline{v} \\ \underline{H}^{-1}(\underline{\tau} + \underline{\tau}_d - \underline{C}\underline{v} - \underline{g}) \end{bmatrix} \tag{17}$$

3. Automatic Controller Design

In this paper, we have tried to control the state vector \underline{q}_n for the robot so that the robot follows the desired path \underline{q}_r . According to Equation (11), the state vector \underline{q}_n must be adjusted and controlled to follow the desired path. To achieve this goal, two kinematic controls and dynamic controls have been used.

Kinematic control is a control rule for Equation (5) whose output is \underline{v}_c vector. This vector is adjusted so that the state vector \underline{q}_n converges to the desired path \underline{q}_r . Dynamic control creates the input signal so that the state vector \underline{v} converges to \underline{v}_c vector. The novelty of this paper is to provide a new dynamic control, which will be discussed in the following sections.

3.1. Kinematic Control

The kinematic control is a loop in the overall control system and is included in most wheeled robot control designs. The error vector is defined as given in Equation (18).

$$\begin{aligned} \tilde{E}_q &= \underline{q}_r - \underline{q}_n \\ &= [x_r - x \quad y_r - y \quad \varphi_r - \varphi \quad \theta_{1r} - \theta_1 \quad \theta_{2r} - \theta_2]^T \end{aligned} \tag{18}$$

where \underline{q}_r is the desired path that the robot should follow.

The goal of the controller is to satisfy $\tilde{E}_q \rightarrow 0$.

Due to the fact that the moving body has movement constraints, its control also requires a separate method. Thus, the error vector is divided into the moving body error vector \tilde{E}_{qB} and the arm error vector \tilde{E}_{qM} .

$$\tilde{E}_q = \begin{bmatrix} \tilde{E}_{qB}^T & \tilde{E}_{qM}^T \end{bmatrix}^T \tag{19}$$

where $\tilde{E}_{qB} = [x_r - x \quad y_r - y \quad \varphi_r - \varphi]^T$ and $\tilde{E}_{qM} = [\theta_{1r} - \theta_1 \quad \theta_{2r} - \theta_2]^T$. Moreover, the robot velocity vector of the robot \underline{v} is divided into two state vectors of the velocity of the wheels of the moving body \bar{v}_w and the velocity vector of the rotational joints of the arm \bar{v}_M .

$$\underline{v} = [\bar{v}_W^T \quad \bar{v}_M^T]^T \tag{20}$$

in which $\bar{v}_w = [\dot{\theta}_R \quad \dot{\theta}_L]^T$ and $\bar{v}_M = [\dot{\theta}_1 \quad \dot{\theta}_2]^T$.

The method utilized in [24] was used to control the moving body. The method used in this study is model-free neuro-fuzzy controller (NFC). This study was performed in order to optimize the parameters and to simplify the design of power system stabilizers (PSSs). According to the results obtained in this study, it has been observed that the mentioned method has a better performance. The velocity of a moving body is defined as Equation (21).

$$\bar{v}_B = [v_b \quad \omega_b]^T \tag{21}$$

where v_b is the size of linear velocity and ω_b is angular velocity. The body velocity \bar{v}_B is related to the wheel speed \bar{v}_w as,

$$\bar{v}_W = \mathbf{T}_B \bar{v}_B = \begin{bmatrix} \frac{1}{r} & \frac{b}{r} \\ \frac{1}{r} & -\frac{b}{r} \end{bmatrix} \bar{v}_B \tag{22}$$

The error vector in the device connected to the moving body is described in Equation (23).

$$E_{qB} = [e_x \quad e_y \quad e_\varphi]^T = \mathbf{T} \tilde{E}_{qB} = \begin{bmatrix} \cos \varphi & \sin \varphi & 0 \\ -\sin \varphi & \cos \varphi & 0 \\ 0 & 0 & 1 \end{bmatrix} \begin{bmatrix} x_r - x \\ y_r - y \\ \varphi_r - \varphi \end{bmatrix} \tag{23}$$

It is suggested in the method given in [24] that control laws track the path desired by the moving body.

$$\begin{aligned} \bar{v}_{Bc} &= \begin{bmatrix} v_{bc} \\ \omega_{bc} \end{bmatrix} = f_B(v_r, \omega_r, E_{qB}) \\ &= \begin{bmatrix} v_r \cos e_\theta + K_x e_x \\ \omega_r + v_r (K_y e_y + K_\theta \sin e_\theta) \end{bmatrix} \end{aligned} \tag{24}$$

where v_r and ω_r are the desired linear velocity and angular velocity for the robot body and $K_x, K_y, K_\theta > 0$ are constant coefficients. It must be the case that $v_r > 0$ to ensure stability.

Now, by placing the relations (22) and (21) in (20), the kinematic control of the moving body is rewritten as Equation (25).

$$\bar{v}_{Wc} = T_B f_B(v_r, \omega_r, T\tilde{E}_{qB}) \tag{25}$$

Besides, for tracking, the desired path is suggested by the joints of the robot arm of the following control law,

$$\begin{aligned} \bar{v}_{Mc} &= \begin{bmatrix} \dot{\theta}_{1c} \\ \dot{\theta}_{2c} \end{bmatrix} = f_M(\dot{\theta}_{1r}, \dot{\theta}_{2r}, \theta_{1r}, \theta_{2r}, \theta_1, \theta_2) \\ &= \begin{bmatrix} \dot{\theta}_{1r} + \lambda_1(\theta_{1r} - \theta_1) \\ \dot{\theta}_{2r} + \lambda_2(\theta_{2r} - \theta_2) \end{bmatrix} \end{aligned} \tag{26}$$

According to Horowitz, $\lambda_1, \lambda_2 > 0$ must be established to ensure stability [37].

Now, according to Equations (25) and (26), the kinematic control is obtained as Equation (27), where \underline{v}_c is the output vector of the control system.

$$\underline{v}_c = \begin{bmatrix} \dot{\theta}_{Rc} \\ \dot{\theta}_{Lc} \\ \dot{\theta}_{1c} \\ \dot{\theta}_{2c} \end{bmatrix} = \begin{bmatrix} T_B f_B(v_r, \omega_r, T\tilde{E}_{qB}) \\ f_M(\dot{\theta}_{1r}, \dot{\theta}_{2r}, \theta_{1r}, \theta_{2r}, \theta_1, \theta_2) \end{bmatrix} \tag{27}$$

3.2. Dynamic Control

Fuzzy systems have been used in various fields for many years. In type-1 fuzzy systems, the membership degree of fuzzy sets is a scalar number. However, in type-2 (general) fuzzy systems, this membership degree is itself a fuzzy set. By considering the fuzzy set of membership degree as an interval, the interval type-2 fuzzy system was introduced. The presence of uncertainty in systems and the inability to define accurate fuzzy membership functions led to the superiority of type-2 fuzzy system over type-1.

This control plan must meet the conditions of \underline{v} to convergence \underline{v}_c . For this purpose, the robot velocity error vector is defined as Equation (28).

$$\tilde{E}_v = \underline{v}_c - \underline{v} = [e_{v1} \quad \dots \quad e_{v4}]^T \tag{28}$$

The fuzzy control scheme consists of 4 interval type-2 fuzzy systems of the Mamdani type. Each fuzzy system has 4 inputs that are included. The membership function was designed for inputs as following equations (see Figure 2).

$$\mu_{Zi^L}(x) = \begin{cases} \frac{0.8(x-a_1^L)}{a_2^L-a_1^L} & \text{if } a_1^L \leq x \leq a_2^L \\ 0.8 & \text{if } a_2^L \leq x \leq a_3^L \\ \frac{0.8(a_4^L-x)}{a_4^L-a_3^L} & \text{if } a_3^L \leq x \leq a_4^L \\ 0 & \text{otherwise} \end{cases} \tag{29}$$

$$\mu_{Zi^U}(x) = \begin{cases} \frac{(x-a_1^U)}{a_2^U-a_1^U} & \text{if } a_1^U \leq x \leq a_2^U \\ 1 & \text{if } a_2^U \leq x \leq a_3^U \\ \frac{(a_4^U-x)}{a_4^U-a_3^U} & \text{if } a_3^U \leq x \leq a_4^U \\ 0 & \text{otherwise} \end{cases} \tag{30}$$

where $x = e_{vi} \ i = 1, \dots, 4$ represents the input number. The output membership functions are defined as follows.

$$\mu_{SM.k}(x) = \exp(-(u_k - u_{FSMC.k})^2/32) \tag{31}$$

$$\mu_{AL.k}(x) = \exp(-(u_k - u_{ALC.k})^2/32) \tag{32}$$

where $k = 1, \dots, 4$ represents the fuzzy system number. The adaptive linear control signal is denoted by u_{ALC} and u_{FSMC} is the control signal from the fuzzy sliding mode controller.

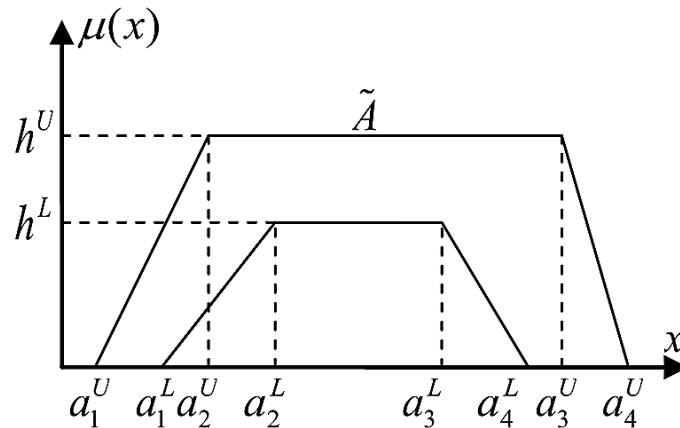


Figure 2. Membership function of the type-2 fuzzy system’s input.

The control strategy is such that the control of the fuzzy sliding mode takes the robot velocity state to a certain neighborhood of the desired state vector. In the optimal state neighborhood, adaptive linear control ensures convergence to the optimal state. For this purpose, each fuzzy system consists of 2 rules.

- Rule 1 : if e_1 is \tilde{Z}_1 and ... e_4 is \tilde{Z}_4 then u_k is AL_k
- Rule 2 : if e_1 is not \tilde{Z}_1 or ... e_4 is not \tilde{Z}_4 then u_k is FSM_k

Using the Mamdani inference system [38], single fuzzy generator, and non-fuzzy center averaging, the output signal of the fuzzy system is obtained as Equation (33).

$$u_k = u_{ALC.k} \left(\frac{\psi_1^L(\tilde{E}_v) + \psi_1^U(\tilde{E}_v)}{2} \right) + u_{FSMC.k} \left(\frac{\psi_2^L(\tilde{E}_v) + \psi_2^U(\tilde{E}_v)}{2} \right) \tag{33}$$

where $\psi_1^L(\tilde{E}_v) = \prod_{i=1}^4 \mu_{Zi^L}(e_{vi})$, $\psi_2^L(\tilde{E}_v) = 1 - \prod_{i=1}^4 \mu_{Zi^L}(e_{vi})$, $\psi_1^U(\tilde{E}_v) = \prod_{i=1}^4 \mu_{Zi^U}(e_{vi})$, $\psi_2^U(\tilde{E}_v) = 1 - \prod_{i=1}^4 \mu_{Zi^U}(e_{vi})$. In the following subsections, we examine fuzzy sliding mode control and adaptive linear control. Figure 2 shows the membership function of the type-2 fuzzy system’s input.

3.3. Type-2 Fuzzy Sliding Mode Control

To design a fuzzy sliding mode controller, the robot model was considered as Equation (34).

$$\dot{v} = f_s + g_s \tau_i \tag{34}$$

where $f_s = \bar{H}^{-1}(\tau_{dis}(t) - \bar{C}v - \bar{g})$ and $g_s = \bar{H}^{-1}$. Proportionally integral is suggested for the sliding surface.

$$s = [s_1 \quad \dots \quad s_4]^T = \tilde{E}_v + \beta \int \tilde{E}_v dt \tag{35}$$

where β is an integral coefficient and must be $\beta > 0$ according to the Horowitz criterion for convergence. The mode path in the tracking coordinate device must be directed to the sliding surface. A certain positive function can be proposed as Equation (35).

$$V_s(s) = 0.5s^T s \tag{36}$$

If the condition $\dot{V}_s(s) \leq 0$ can be guaranteed, then $V_s(s) \rightarrow 0$ can be guaranteed. By derivative of Equation (36),

$$\dot{V}_s(s) = \dot{s}^T s \tag{37}$$

Therefore, the following condition must be met to converge.

$$\dot{s}^T (s / \|s\|) \leq -\eta \tag{38}$$

where η is a positive constant. By placing the derivative of (37) in Equation (38),

$$\left(\dot{v}_c - \underline{v} + \beta \tilde{E}_v\right)^T (s / \|s\|) \leq -\eta \tag{39}$$

Now, substituting Equation (34) into Equation (39) so that the controller output appears in the equations,

$$\left(\dot{v}_c - f_s - g_s \tau_i + \beta \tilde{E}_v\right)^T (s / \|s\|) \leq -\eta \tag{40}$$

The limitation of the system state variables is demonstrated. Suppose f_s is limited, i.e.,

$$\|f_s\| \leq F \tag{41}$$

where F is a positive constant. Taking $\gamma_s = \eta + F$, the sliding mode control is calculated as Equation (42).

$$u = g_s^{-1} \left(\dot{v}_c + \gamma_s \text{sgn}(s) + \beta \tilde{E}_v \right) \tag{42}$$

where $\text{sgn}(s) = [\text{sgn}(s_1) \dots \text{sgn}(s_4)]^T$ is the sign function. In order to reduce the control signal vibration, the fuzzy form of the sign function was used.

$$u_{FSMC} = g_s^{-1} \left(\dot{v}_c + \beta \tilde{E}_v + u_{FSGN} \right) \tag{43}$$

If by applying a constraint, the output of the controller exceeds the maximum torque value, the controller is practically out of the circuit, and only the maximum torque is applied.

To create u_{FSGN} , 4 interval type-2 fuzzy systems of the Mamdani type are used. Each of them is single input single output. The membership function was designed for inputs as given by the following equations.

$$\mu_{P_j^L}(s_j) = \begin{cases} \frac{0.8(s_j - b_1^L)}{b_2^L - b_1^L} & \text{if } b_1^L \leq s_j \leq a_2^L \\ 0.8 & \text{if } b_2^L \leq s_j \leq b_3^L \\ \frac{0.8(b_4^L - s_j)}{b_4^L - b_3^L} & \text{if } b_3^L \leq s_j \leq b_4^L \\ 0 & \text{otherwise} \end{cases} \tag{44}$$

$$\mu_{P_j^U}(s_j) = \begin{cases} \frac{(s_j - b_1^U)}{b_2^U - b_1^U} & \text{if } b_1^U \leq s_j \leq b_2^U \\ 1 & \text{if } b_2^U \leq s_j \leq b_3^U \\ \frac{(b_4^U - s_j)}{b_4^U - b_3^U} & \text{if } b_3^U \leq s_j \leq b_4^U \\ 0 & \text{otherwise} \end{cases} \tag{45}$$

where $s_j, j = 1, \dots, 4$ represents the input number. The output membership functions are defined as follows,

$$\mu_{\text{FSGN},j}(x) = \exp\left(-\left(u_j - u_{\text{FSGN},j}\right)^2/32\right) \tag{46}$$

where $j = 1, \dots, 4$ represents the fuzzy system number. Each fuzzy system has the following form.

$$\text{Rule } j : \text{ if } s_j \text{ is } \tilde{P}_j \text{ then } u_{\text{FSGN},j} \text{ is } \tilde{N}_j$$

Both \tilde{P}_j and \tilde{N}_j are type-1 fuzzy number. Using the Mamdani inference system [34], single fuzzy generator, and non-fuzzy center averaging, the output signal of the fuzzy system is obtained as Equation (47).

$$u_{\text{FSGN}} = \sum_{j=1}^4 u_{\text{FSGN},j} \left(\frac{\psi_1^L(\tilde{E}_v) + \psi_1^U(\tilde{E}_v)}{2} \right) \tag{47}$$

where $\psi_1^L(s_j) = \prod_{l=1}^4 \mu_{P_l}(s_j) \mu_{\text{FSGN},j}(u_{\text{FSGN},j})$, $\psi_1^U(s_j) = \prod_{l=1}^4 \mu_{P_l^U}(s_j) \mu_{\text{FSGN},j}(u_{\text{FSGN},j})$.

3.4. Adaptive Linear Control

To define the adaptive linear control, the following vector is defined.

$$E = \underline{X}_d - \underline{X} = \left[(\underline{v}_c - \underline{v})^T \quad (\underline{q}_r - \underline{q}_n)^T \right]^T = \left[\tilde{E}_v^T \quad \tilde{E}_q^T \right]^T \tag{48}$$

The goal of the controller is $E \rightarrow 0$. Assuming that there is no perturbation, Equation (48) is modified as Equation (49).

$$\underline{H}(\underline{q}_n) \dot{\underline{v}} + \underline{C}(\underline{q}_n, \underline{v}) \underline{v} + \underline{g}(\underline{q}_n) = \underline{\tau} \tag{49}$$

With linearization of (48) around the equilibrium point $E = 0$,

$$-A_3 \dot{\tilde{E}}_v = \underline{\tau} - \tau_d + A_1 \tilde{E}_q + A_2 \tilde{E}_v \tag{50}$$

where $A_1 = \left(\frac{\partial \underline{H}}{\partial \underline{q}_n} + \frac{\partial \underline{C}}{\partial \underline{q}_n} + \frac{\partial \underline{g}}{\partial \underline{q}_n} \right) \Big|_{x_d}$, $A_2 = \left(\underline{C} + \frac{\partial \underline{C}}{\partial \underline{v}} \right) \Big|_{x_d}$, $A_3 = \underline{H}|_{x_d}$ and $\tau_d = \underline{H}(\underline{q}_r) \dot{\underline{v}}_c + \underline{C}(\underline{q}_r, \underline{v}_c) + \underline{g}$, as recommended for the following control law:

$$\underline{\tau} = C_1 \tilde{E}_q + C_2 \tilde{E}_v + C_0 \tag{51}$$

By applying the control law (51) to Equation (50), we obtain:

$$\dot{\tilde{E}}_v = A_3^{-1} \left((\tau_d - C_0) - (A_1 + C_1) \tilde{E}_q - (A_2 + C_2) \tilde{E}_v \right) \tag{52}$$

Assuming $C_0 = \tau_d$ and $C_1 = -A_1$, Equation (52) is simplified as follows:

$$\dot{\tilde{E}}_v + A_3^{-1} (A_2 + C_2) \tilde{E}_v = 0 \tag{53}$$

Assuming $A_3^{-1} (A_2 + C_2) = \bar{K}$ and \bar{K} is Horowitz matrix, $\tilde{E}_v \rightarrow 0$ is also established. According to the kinematic control $\tilde{E}_q \rightarrow 0$ is also achieved. So, with the above assumptions,

$E \rightarrow 0$ is established. Suppose that control of (53) in the equilibrium point sets the velocity vector convergence conditions for model of (49).

$$\begin{aligned} \underline{H}(q_n)\dot{v}_c + \underline{C}(q_n, v)v_c + \underline{g}(q_n) - \bar{\tau}_d + \bar{K}\tilde{E}_v \\ = C_1\tilde{E}_q + (C_2 + \bar{K})\tilde{E}_v + C_0 \\ = K_1\tilde{E}_q + K_2\tilde{E}_v + K_0 \end{aligned} \tag{54}$$

Equation (54) can be rewritten as a linear combination of parameters as follows:

$$\begin{aligned} \underline{H}(q_n)\dot{v}_c + \underline{C}(q_n, v)v_c + \underline{g}(q_n) - \bar{\tau}_d + \bar{K}\tilde{E}_v \\ = Y(\tilde{E}_q, \tilde{E}_v)P \end{aligned} \tag{55}$$

where $Y(\tilde{E}_q, \tilde{E}_v)$ is the regression matrix and P is the parameter matrix. The law of adaptive linear control is presented as follows:

$$\underline{\tau} = \hat{K}_1\tilde{E}_q + \hat{K}_2\tilde{E}_v + \hat{K}_0 = Y(\tilde{E}_q, \tilde{E}_v)\hat{P} \tag{56}$$

By applying (52) to model of (56), we get:

$$\underline{H}(q_n)\dot{v} + \underline{C}(q_n, v)v + \underline{g}(q_n) - \bar{\tau}_d = Y(\tilde{E}_q, \tilde{E}_v)\hat{P} \tag{57}$$

Using the previous relations, we can write Equation (58) as follows:

$$\begin{aligned} \underline{H}(q_n)\dot{\tilde{E}}_v + \underline{C}(q_n, v)\tilde{E}_v + \bar{K}\tilde{E}_v = Y(\tilde{E}_q, \tilde{E}_v)(P - \hat{P}) \\ = Y(\tilde{E}_q, \tilde{E}_v)\hat{P} \end{aligned} \tag{58}$$

A certain positive function V can be suggested as follows:

$$V = 0.5\tilde{E}_v^T \underline{H}(q_n)\tilde{E}_v + 0.5\tilde{P}^T \tilde{P} / \gamma \tag{59}$$

Derived from (59), we have:

$$\dot{V} = \tilde{E}_v^T \underline{H}(q_n)\dot{\tilde{E}}_v + 0.5\tilde{E}_v^T \dot{\underline{H}}(q_n)\tilde{E}_v - \dot{\tilde{P}}^T \tilde{P} / \gamma \tag{60}$$

Then, we can obtain:

$$\begin{aligned} \dot{V} = \tilde{E}_v^T \left(-\underline{C}(q_n, v)\tilde{E}_v - \bar{K}\tilde{E}_v + Y(\tilde{E}_q, \tilde{E}_v)\tilde{P} \right) \\ + 0.5\tilde{E}_v^T \dot{\underline{H}}(q_n)\tilde{E}_v - \dot{\tilde{P}}^T \tilde{P} / \gamma \end{aligned} \tag{61}$$

With simplification, the above equation becomes:

$$\begin{aligned} \dot{V} = -\tilde{E}_v^T \bar{K}\tilde{E}_v + 0.5\tilde{E}_v^T (\underline{H}(q_n) - 2\underline{C}(q_n, v))\tilde{E}_v \\ + \left(\tilde{E}_v^T Y(\tilde{E}_q, \tilde{E}_v) - \dot{\tilde{P}}^T / \gamma \right) \tilde{P} \\ = -\tilde{E}_v^T \bar{K}\tilde{E}_v + \left(\tilde{E}_v^T Y(\tilde{E}_q, \tilde{E}_v) - \dot{\tilde{P}}^T / \gamma \right) \tilde{P} \end{aligned} \tag{62}$$

So, it is obtained $\dot{\hat{P}}^T = \gamma \tilde{E}_v^T \Upsilon (\tilde{E}_q, \tilde{E}_v)$ by zeroing $\tilde{E}_v^T \Upsilon (\tilde{E}_q, \tilde{E}_v) - \frac{\dot{\hat{P}}^T}{\gamma} = 0$, so the adaptation law can be written as Equation (63).

$$\hat{P}(t) = \int \gamma \Upsilon (\tilde{E}_q, \tilde{E}_v)^T \tilde{E}_v dt \tag{63}$$

Finally, we have:

$$\dot{V} = -\tilde{E}_v^T \bar{K} \tilde{E}_v \leq 0 \tag{64}$$

$\tilde{E}_v \rightarrow 0$ is proved according to Lyapanov theory. Given that $\dot{V} \leq 0$, at all times, we have:

$$V(\tilde{E}_v, \tilde{P}) \leq V(\tilde{E}_v(0), \tilde{P}(0)) \tag{65}$$

Thus, \tilde{E}_v and \tilde{P} are limited. It can also be claimed that v is limited by v_c being limited. So, all system state variables are also limited, implying that the stable system is of limited input-output type.

4. Simulation Results

In this section, to evaluate the performance of the adaptive fuzzy control scheme, the proposed control law is applied to the wheeled mobile arm and its performance is compared with the robust adaptive control (RAC) method of [3]. The kinematic and dynamic parameters of the robot are given in Tables 1 and 2, respectively. In Table 1, It is assumed that the mass of the link is spread uniformly along its length. The parameters of kinematic and dynamic controllers are given in Tables 3 and 4, respectively. In order to ensure stability according to the Horowitz criteria as described in Section 3, it must be the case that $\lambda_1, \lambda_2 > 0$ established in the kinematic controller. The constant parameters of the controllers are obtained following the trial-and-error method to achieve the desired performance in the simulation. The initial value of the zero adaptive parameters is selected and the fuzzy controller parameters are comparatively calculated from expressed equations. The proposed control is continuous and usually the data collection time in the digital control is specified for the digital control. The robot corresponding to the proposed design has a suitable data collection frequency of 200 Hz. The robot at the beginning of the movement is $X(0) = 0$. According to the previous equations, the optimal path can be written as follows:

$$\begin{aligned} X_d(t) &= 2 \cos(\omega_1 t), Y_d(t) = 2 \sin(\omega_1 t) \\ \theta_1(t) &= 2 \sin(\omega_2 t), \theta_2(t) = 2 \cos(\omega_2 t) \\ \varphi_d(t) &= \omega_1 t + \pi/2 \end{aligned} \tag{66}$$

where $\omega_1 = 0.1$ and $\omega_2 = 0.4$ and the initial values of path (68) are $X_d(0) = 2, Y_d(0) = 0, \theta_1(0) = 0, \theta_2(0) = 2$ and $\varphi_d(0) = \pi/2$. Perturbation is defined as follows:

$$\bar{\tau}_d(t) = 1.5[\sin(0.6t) \cos(0.6t) 2 \sin(0.3t) 2 \cos(0.3t)]^T$$

Table 1. Robot kinematic parameters [39–41].

Parameter	Description	Value (m)
b	The distance of wheel to the robot center line	0.180
d	The distance of wheels axis and robot center of mass	0.115
r	Wheel radius	0.05
L_a	The distance of point P to the robot center of mass	0.1
L_1	Link 1 length	0.15
L_2	Link 2 length	0.1
L_{cm1}	Location of the link 1 center of mass	0.075
L_{cm2}	Location of the link 2 center of mass	0.05

Table 2. Robot dynamic parameters.

Parameter	Description	Value
I_w	Wheel inertia	0.0002 kg.m ²
m_w	The mass of wheel	0.160 kg
I_c	Body inertia in Z direction	0.280 kg.m ²
m_c	The mass of body	0.1 kg
I_1	Link 1 inertia in Z direction	0.15 kg.m ²
m_1	The mass of link 1	0.1 kg
I_2	Link 2 inertia in X/Y directions	0.075 kg.m ²
m_2	The mass of link 2	0.05 kg

Table 3. Kinematic control parameters.

K_x	K_y	K_θ	λ_1	λ_2
10	20	0.01	10	10

Table 4. Dynamic control parameters.

γ	τ_{max}	b_{vc}	b_{vs}	P	L	K
10 0	$\begin{bmatrix} 30 \\ 30 \\ 10 \\ 10 \end{bmatrix}$	$\begin{bmatrix} 2.5 \\ 2.5 \\ 2 \\ 2 \end{bmatrix}$	$\begin{bmatrix} 0.1 \\ 0.1 \\ 1 \\ 1 \end{bmatrix}$	I_{4*4}	I_{9*9}	$diag(0.1, 0.1, 1, 1)$

Figure 3a shows the performance of controllers in tracking with a moving body. Both controllers perform well. The magnitude of the tracking error to check the performance of the proposed controller is plotted in Figure 3b. The size of the body position tracking error starts from 2 m and in the presence of uncertainty, it converges to zero asymptotically, which shows the ability of the fuzzy system to overcome uncertainty. The tracking performance of the two controllers for the angle of the second joint of the arm is compared in Figure 4. As can be seen, the two controllers are quickly converged to the desired path with the help of the same kinematic control with a small error. The magnitude of the second arm joint position tracking error to plot the performance of the proposed controller (AFC) is plotted in Figure 5. The magnitude of the error starts from 2 radians and converges to zero in the presence of uncertainty, which shows the ability of the fuzzy system to overcome uncertainty. Figure 6 shows the error rate of the robot speed tracking by two controllers. In this comparison, the proposed controller (AFC) performed much better than the RAC, and the tracking error rate was asymptotically converged to zero. The control signals of AFC and RAC are compared in Figures 7 and 8 and the superiority of the proposed method can be seen.

Initially, due to the type-2 fuzzy sliding mode operation in the control loop, we have the signal chattering, but with the passage of time and the activation of adaptive linear control, the signal vibration also decreases. Moreover, considering that, in this method, the law of linear control matching when the error range is small is activated, there are no rapid changes in the matching parameters, so with the jump of the control signal, the installation is reduced in another way. The control effort of the RAC in the initial moments is large, which creates a problem for the robot’s motions, but this problem has been solved despite the limiting function in the proposed scheme. One of the ways to challenge a control system is by applying a disturbance to the controlled system. Figure 8 shows the performance results of both control systems in facing this challenge.

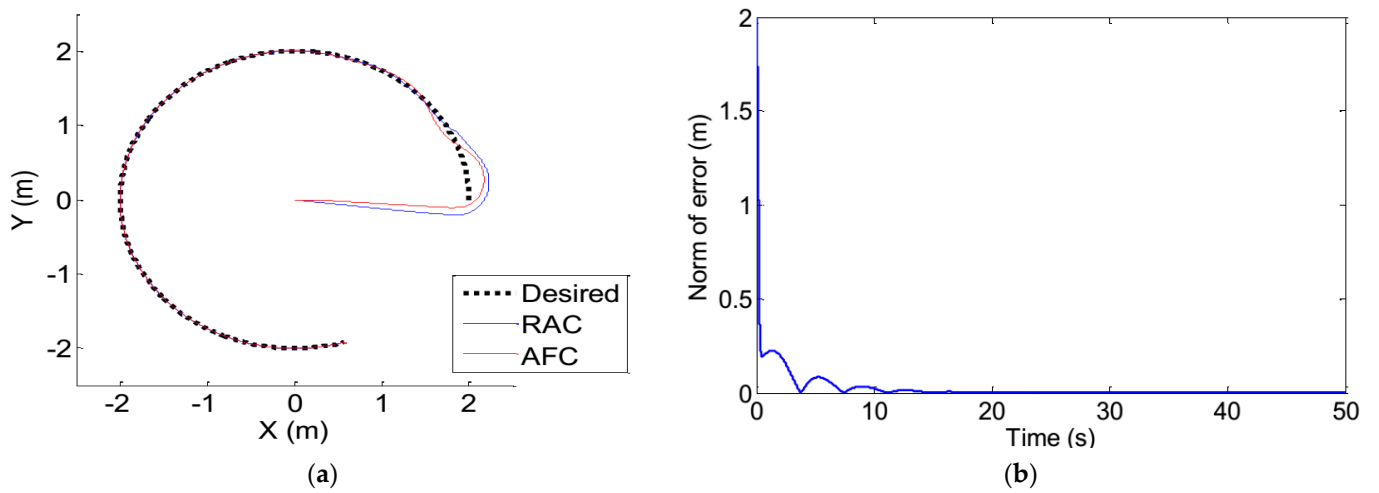


Figure 3. (a) The performance of controllers in tracking by moving body (b) The tracking error magnitude of the proposed method.

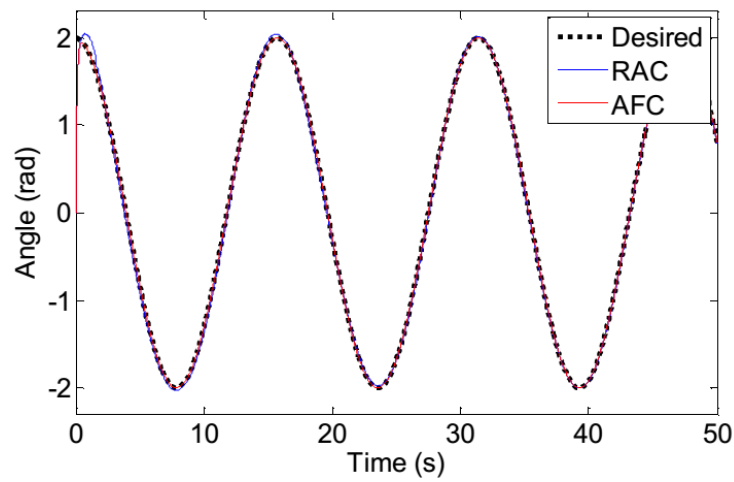


Figure 4. The tracking performance of the two controllers for the angle of the second joint of the arm.

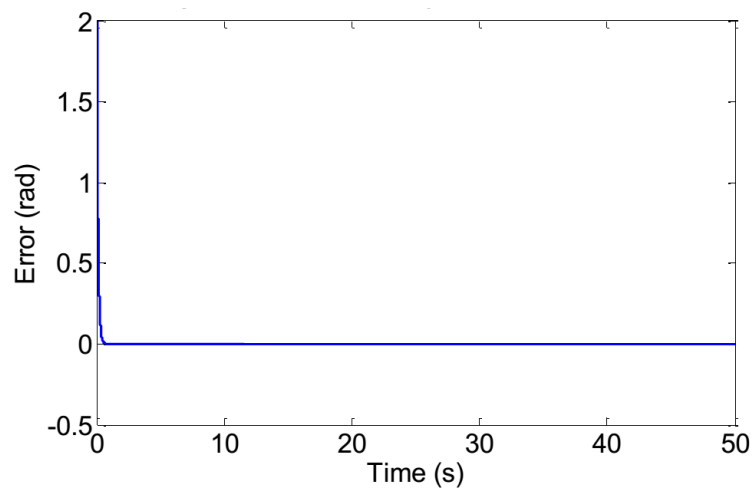


Figure 5. The magnitude of the second arm joint position tracking error.

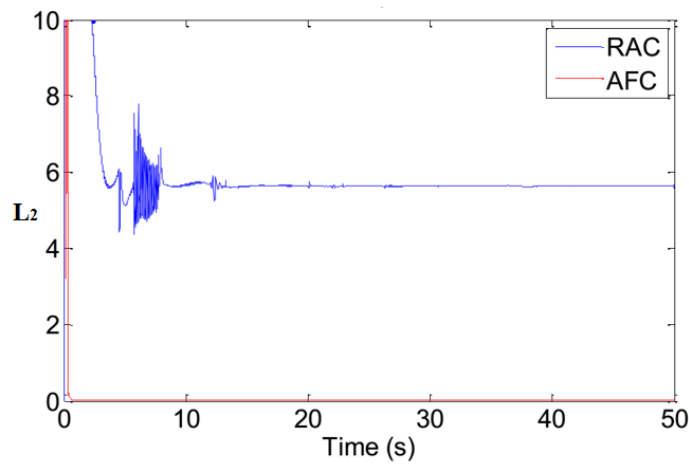


Figure 6. The magnitude of robot velocity error based on AFC and RAC.

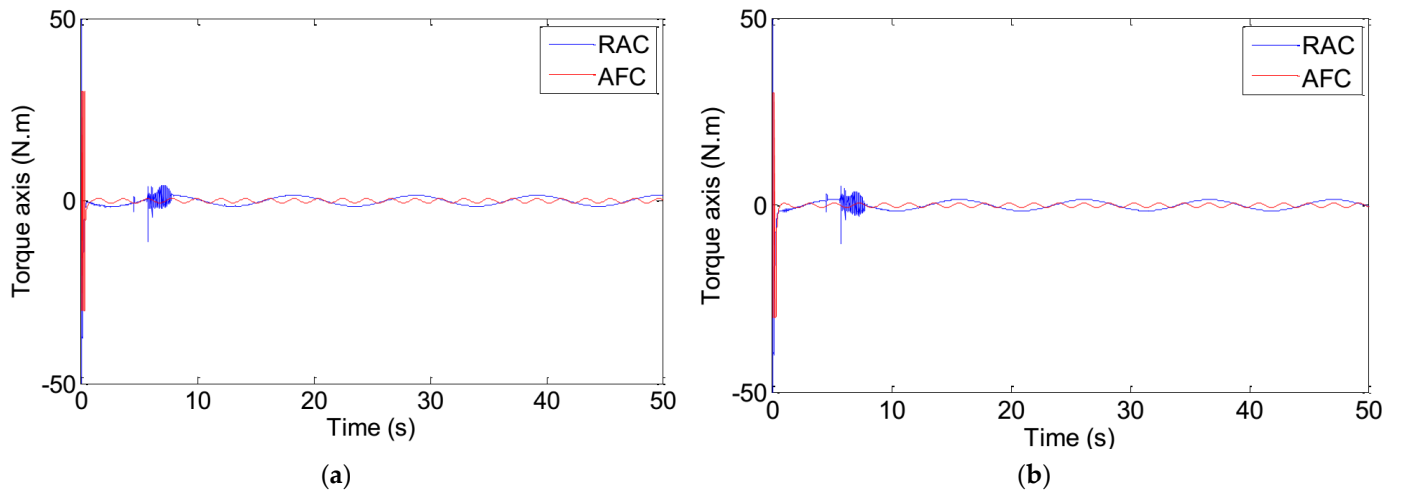


Figure 7. (a) Right wheel control signal and (b) Left wheel control signal.

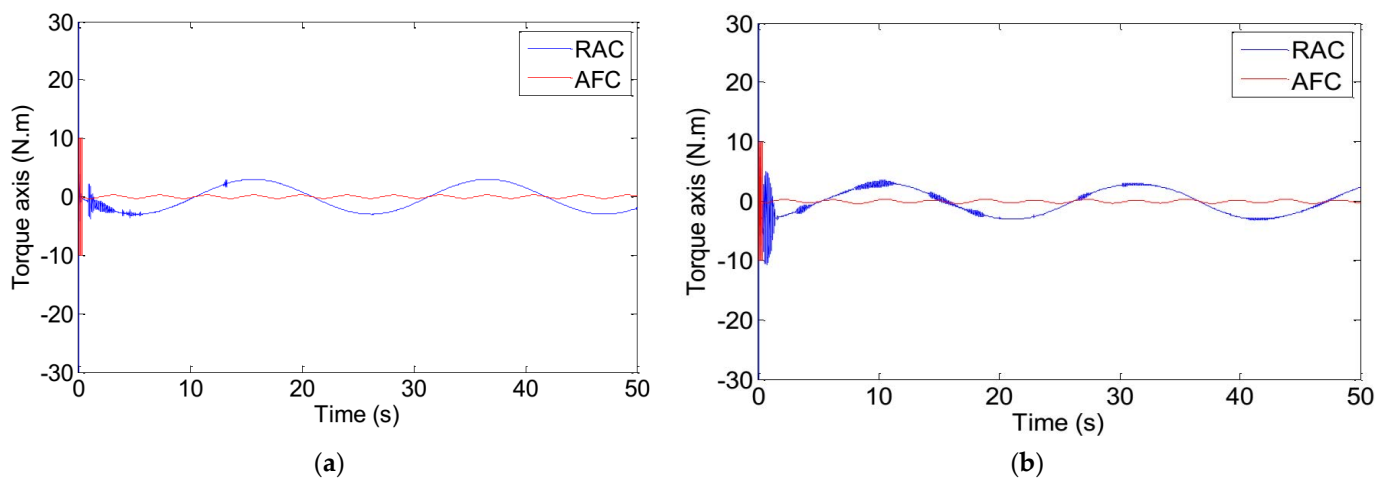


Figure 8. (a) First joint control signal and (b) Second joint control signal.

In Figure 9, at point $x = 1$ m, a wind disturbance force of 1 N/m is applied in the right direction, and at point $x = 2$ m, a force of 0.5 N/m is applied to the robot in the left direction. As can be seen, the proposed control system has a better performance and has guided the robot to the desired path at a faster speed. In order to further compare the performance of the proposed method with other methods, as presented in Table 5, two measures of

root mean squares error (RMSE) and step response time are calculated. As can be seen in Table 5, the proposed control system has shown a much better performance than the methods presented in [29,30] in both the RMSE and the step response time (response speed) as measurement criteria.

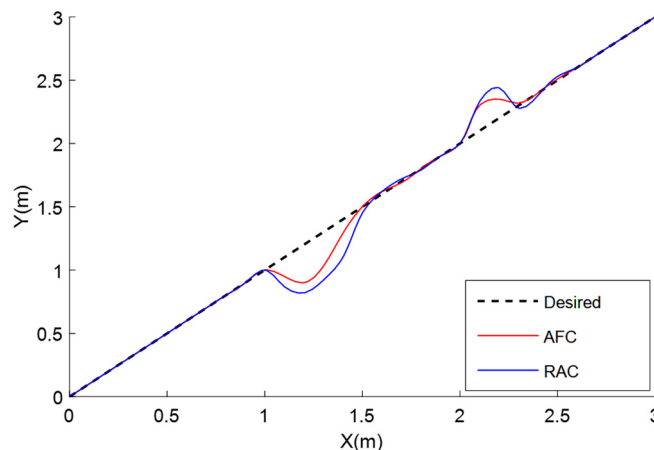


Figure 9. Apply disturbances as an obstacle in the path of the robot.

Table 5. Comparison based on RMSE and step response time.

	RMSE	Step Response Time (s)
Method of [42]	0.411	1.24
Method of [43]	0.294	1.01
Proposed method	0.153	0.83

5. Conclusions

In this paper, dynamic modeling of a non-holonomic wheeled robotic arm and a new method of adaptive fuzzy control for a mobile robotic arm were presented. The proposed scheme is used to compensate for the approximation error of the adaptive fuzzy system, to achieve asymptotic convergence to follow the desired path in the existence of uncertainties. The stability of the control system and the convergence of the path to the desired path were proved by the Lyapunov method. The advantages of the proposed design are the simplicity of design and proper performance in following the desired path in the presence of uncertainties. Our model gave an RMSE of 0.153, while the step response time was only 0.83 s. The simulation results show the superiority of the proposed design over a robust adaptive control method.

Author Contributions: Conceptualization, X.X. and A.S.; methodology, X.X.; software, X.X.; validation, X.X., A.S. and M.S.S.; formal analysis, X.X.; investigation, X.X. and M.S.S.; resources, X.X. and M.S.S.; data curation, X.X.; writing—original draft preparation, X.X.; writing—review and editing, X.X., A.S. and M.S.S. All authors have read and agreed to the published version of the manuscript.

Funding: This research received no external funding.

Data Availability Statement: Not applicable.

Conflicts of Interest: The authors declare no conflict of interest.

References

1. Yang, L.; Guo, M.; Mohammadzadeh, A.; Mosavi, A. Taylor Series-Based Fuzzy Model Predictive Control for Wheeled Robots. *Mathematics* **2022**, *10*, 2498. [\[CrossRef\]](#)
2. Huang, H.; Shirkhani, M.; Tavoosi, J.; Mahmoud, O. A New Intelligent Dynamic Control Method for a Class of Stochastic Nonlinear Systems. *Mathematics* **2022**, *10*, 1406. [\[CrossRef\]](#)
3. Li, X.; Yang, X.; Zhang, C.; Qi, M. A simulation study on the robotic mobile fulfillment system in high-density storage warehouses. *Simul. Model. Pract. Theory* **2021**, *112*, 102366. [\[CrossRef\]](#)

4. Dörfler, K.; Hack, N.; Sandy, T.; Gifftthaler, M.; Lussi, M.; Walzer, A.N.; Buchli, J.; Gramazio, F.; Kohler, M. Mobile robotic fabrication beyond factory conditions: Case study Mesh Mould wall of the DFAB HOUSE. *Constr. Robot.* **2019**, *3*, 53–67. [[CrossRef](#)]
5. Tavooosi, J.; Shirkhani, M.; Abdali, A.; Mohammadzadeh, A.; Nazari, M.; Mobayen, S.; Asad, J.H.; Bartoszewicz, A. A New General Type-2 Fuzzy Predictive Scheme for PID Tuning. *Appl. Sci.* **2021**, *11*, 10392. [[CrossRef](#)]
6. Ha, Q.P.; Yen, L.; Balaguer, C. Robotic autonomous systems for earthmoving in military applications. *Autom. Constr.* **2019**, *107*, 102934. [[CrossRef](#)]
7. Gopinath, A.; Jisha, V.R. Gain Scheduled LQR Control of a Two Wheeled Mobile Robot with Heavy Payloads. In Proceedings of the 2022 IEEE International Conference on Signal Processing, Informatics, Communication and Energy Systems (SPICES), Trivandrum, India, 10 March 2022; Volume 1, pp. 436–441.
8. Nath, K.; Yesmin, A.; Nanda, A.; Bera, M.K. Event-triggered sliding-mode control of two wheeled mobile robot: An experimental validation. *IEEE J. Emerg. Sel. Top. Ind. Electron.* **2021**, *2*, 218–226. [[CrossRef](#)]
9. Hyatt, P.; Wingate, D.; Killpack, M.D. Model-based control of soft actuators using learned non-linear discrete-time models. *Front. Robot. AI* **2019**, *6*, 22. [[CrossRef](#)]
10. Hsu, Y.S.; Chen, Y.P.; Shaffer, M.A. Reducing work and home cognitive failures: The roles of workplace flextime use and perceived control. *J. Bus. Psychol.* **2021**, *36*, 155–172. [[CrossRef](#)]
11. Mobayen, S.; Ma, J. Robust finite-time composite nonlinear feedback control for synchronization of uncertain chaotic systems with nonlinearity and time-delay. *Chaos Solitons Fractals* **2018**, *114*, 46–54. [[CrossRef](#)]
12. Xing, X.; Liu, J. Robust adaptive control allocation for a class of cascade ODE-string systems with actuator failures. *IEEE Trans. Autom. Control* **2021**, *67*, 1474–1481. [[CrossRef](#)]
13. Mohammadi, F.; Mohammadi-Ivatloo, B.; Gharehpetian, G.B.; Ali, M.H.; Wei, W.; Erding, O.; Shirkhani, M. Robust control strategies for microgrids: A review. *IEEE Syst. J.* **2021**, *16*, 2401–2412. [[CrossRef](#)]
14. Ren, Y.; Wang, R.; Rind, S.J.; Zeng, P.; Jiang, L. Speed sensorless nonlinear adaptive control of induction motor using combined speed and perturbation observer. *Control Eng. Pract.* **2022**, *123*, 105166. [[CrossRef](#)]
15. Danyali, S.; Aghaei, O.; Shirkhani, M.; Aazami, R.; Tavooosi, J.; Mohammadzadeh, A.; Mosavi, A. A New Model Predictive Control Method for Buck-Boost Inverter-Based Photovoltaic Systems. *Sustainability* **2022**, *14*, 11731. [[CrossRef](#)]
16. Chen, H.; Fang, Y.; Sun, N. An adaptive tracking control method with swing suppression for 4-DOF tower crane systems. *Mech. Syst. Signal Process.* **2019**, *123*, 426–442. [[CrossRef](#)]
17. Roy, S.; Lee, J.; Baldi, S. A new adaptive-robust design for time delay control under state-dependent stability condition. *IEEE Trans. Control Syst. Technol.* **2020**, *29*, 420–427. [[CrossRef](#)]
18. Wang, H.; Liu, P.X.; Bao, J.; Xie, X.J.; Li, S. Adaptive neural output-feedback decentralized control for large-scale nonlinear systems with stochastic disturbances. *IEEE Trans. Neural Netw. Learn. Syst.* **2019**, *31*, 972–983. [[CrossRef](#)] [[PubMed](#)]
19. Fei, J.; Chen, Y.; Liu, L.; Fang, Y. Fuzzy multiple hidden layer recurrent neural control of nonlinear system using terminal sliding-mode controller. *IEEE Trans. Cybern.* **2021**, *52*, 9519–9534. [[CrossRef](#)]
20. Chertopolokhov, V.; Andrianova, O.; Hernandez-Sanchez, A.; Mireles, C.; Poznyak, A.; Chairez, I. Averaged sub-gradient integral sliding mode control design for cueing end-effector acceleration of a two-link robotic arm. *ISA Trans.* **2022**. [[CrossRef](#)] [[PubMed](#)]
21. Cruz-Ortiz, D.; Chairez, I.; Poznyak, A. Adaptive sliding-mode trajectory tracking control for state constraint master-slave manipulator systems. *ISA Trans.* **2022**, *127*, 273–282. [[CrossRef](#)]
22. Chairez, I.; Utkin, V. Electrocardiographically Signal Simulator Based on a Sliding Mode Controlled Buck DC-DC Power Converter. *IFAC-PapersOnLine* **2022**, *55*, 419–424. [[CrossRef](#)]
23. Moaveni, B.; Rashidi Fathabadi, F.; Molavi, A. Fuzzy control system design for wheel sliding prevention and tracking of desired speed profile in electric trains. *Asian J. Control* **2022**, *24*, 388–400. [[CrossRef](#)]
24. Sabo, A.; Abdul Wahab, N.I.; Othman, M.L.; Mohd Jaffar, M.Z.; Beiranvand, H.; Acikgoz, H. Application of a neuro-fuzzy controller for single machine infinite bus power system to damp low-frequency oscillations. *Trans. Inst. Meas. Control* **2021**, *43*, 3633–3646. [[CrossRef](#)]
25. Yonezawa, A.; Yonezawa, H.; Kajiwara, I. Parameter tuning technique for a model-free vibration control system based on a virtual controlled object. *Mech. Syst. Signal Process.* **2022**, *165*, 108313. [[CrossRef](#)]
26. Labiod, S.; Guerra, T.M. Adaptive Fuzzy Control for Multivariable Nonlinear Systems with Indefinite Control Gain Matrix and Unknown Control Direction. *IFAC-PapersOnLine* **2020**, *53*, 8019–8024. [[CrossRef](#)]
27. Zhu, Z.; Pan, Y.; Zhou, Q.; Lu, C. Event-triggered adaptive fuzzy control for stochastic nonlinear systems with unmeasured states and unknown backlash-like hysteresis. *IEEE Transactions on Fuzzy Systems* **2020**, *29*, 1273–1283. [[CrossRef](#)]
28. Rao, V.V.; Kumar, A.A. Artificial neural network and adaptive neuro fuzzy control of direct torque control of induction motor for speed and torque ripple control. In Proceedings of the 2018 2nd International Conference on Trends in Electronics and Informatics (ICOEI), Tirunelveli, India, 11 May 2018; pp. 1416–1422.
29. Anisimov, D.N.; Dang, T.S.; Dinh, V.N. Development of a microcontroller-based adaptive fuzzy controller for a two-wheeled self-balancing robot. *Microsyst. Technol.* **2018**, *24*, 3677–3687.
30. Li, B.; Wang, S.; Fernandez, C.; Yu, C.; Xia, L.; Fan, Y. A linear recursive state of power estimation method based on fusion model of voltage and state of charge limitations. *J. Energy Storage* **2021**, *40*, 102583. [[CrossRef](#)]
31. Aazami, R.; Heydari, O.; Tavooosi, J.; Shirkhani, M.; Mohammadzadeh, A.; Mosavi, A. Optimal Control of an Energy-Storage System in a Microgrid for Reducing Wind-Power Fluctuations. *Sustainability* **2022**, *14*, 6183. [[CrossRef](#)]

32. Iranmehr, H.; Aazami, R.; Tavvoosi, J.; Shirkhani, M.; Azizi, A.R.; Mohammadzadeh, A.; Mosavi, A.H.; Guo, W. Modeling the Price of Emergency Power Transmission Lines in the Reserve Market Due to the Influence of Renewable Energies. *Front. Energy Res.* **2022**, *9*. [[CrossRef](#)]
33. Tavvoosi, J.; Mohammadzadeh, A.; Jermittiparsert, K. A review on type-2 fuzzy neural networks for system identification. *Soft Comput.* **2021**, *25*, 7197–7212. [[CrossRef](#)] [[PubMed](#)]
34. Tavvoosi, J.; Shirkhani, M.; Azizi, A.; Din, S.U.; Mohammadzadeh, A.; Mobayen, S. A hybrid approach for fault location in power distributed networks: Impedance-based and machine learning technique. *Electr. Power Syst. Res.* **2022**, *210*, 108073. [[CrossRef](#)]
35. Janková, Z.; Dostál, P. Type-2 fuzzy expert system approach for decision-making of financial assets and investing under different uncertainty. *Math. Probl. Eng.* **2021**, *2021*, 3839071. [[CrossRef](#)]
36. Tavvoosi, J.; Shirkhani, M.; Azizi, A. Control engineering solutions during epidemics: A review. *Int. J. Model. Identif. Control* **2021**, *39*, 97–106. [[CrossRef](#)]
37. Seeliger, D.; De Groot, B.L. Protein thermostability calculations using alchemical free energy simulations. *Biophys. J.* **2010**, *98*, 2309–2316. [[CrossRef](#)]
38. Rustum, R.; Kurichiyani, A.M.J.; Forrest, S.; Sommariva, C.; Adeloye, A.J.; Zounemat-Kermani, M.; Scholz, M. Sustainability Ranking of Desalination Plants Using Mamdani Fuzzy Logic Inference Systems. *Sustainability* **2020**, *12*, 631. [[CrossRef](#)]
39. Gao, G.; Liu, F.; San, H.; Wu, X.; Wang, W. Hybrid optimal kinematic parameter identification for an industrial robot based on BPNN-PSO. *Complexity* **2018**, *2018*, 4258676. [[CrossRef](#)]
40. He, S.; Ma, L.; Yan, C.; Lee, C.H.; Hu, P. Multiple location constraints based industrial robot kinematic parameter calibration and accuracy assessment. *Int. J. Adv. Manuf. Technol.* **2019**, *102*, 1037–1050. [[CrossRef](#)]
41. Gan, Y.; Duan, J.; Dai, X. A calibration method of robot kinematic parameters by drawstring displacement sensor. *Int. J. Adv. Robot. Syst.* **2019**, *16*, 1729881419883072. [[CrossRef](#)]
42. Brahmi, A.; Saad, M.; Brahmi, B.; Bojairami, I.E.; Gauthier, G.; Ghommam, J. Robust adaptive tracking control for uncertain nonholonomic mobile manipulator. *Proc. Inst. Mech. Eng. Part I J. Syst. Control Eng.* **2022**, *236*, 395–405. [[CrossRef](#)]
43. Leoro, J.; Hsiao, T. Motion Planning of Nonholonomic Mobile Manipulators with Manipulability Maximization Considering Joints Physical Constraints and Self-Collision Avoidance. *Appl. Sci.* **2021**, *11*, 6509. [[CrossRef](#)]